Promising bioactive properties of (2R,5S)-2,5-dimethylpiperazine-1,4-diium dinitrate material: experimental, theoretical and in silico investigation

Sofian Gatfaoui, Noureddine Issaoui, Aleksandr S. Kazachenko, Omar M Al-Dossary, Naveen Kumar Singh, Thierry Roisnel, Houda Marouani, Anna S. Kazachenko, Yuriy N Malyar

Promising bioactive properties of (2R,5S)-2,5-dimethylpiperazine-1,4-diium dinitrate material : experimental, theoretical and in silico investigation

Sofian Gatfaoui [a], Noureddine Issaoui[b*], Aleksandr S. Kazachenko [c,d*], Omar M. Al-Dossary[e], Naveen Kumar[f], Thierry Roisnel [g], Houda Marouani [a], Anna S. Kazachenko [c] and Yuriy N. Malyar[c,d]

[a]Materials Chemistry Laboratory, Faculty of Sciences of Bizerte, Carthage University, 7021 Zarzouna, Tunisia.
[b]Laboratory of Quantum and Statistical Physics (LR18ES18), Faculty of Sciences, University of Monastir, Monastir 5000, Tunisia;
[c]Siberian Federal University, pr. Svobodny 79, Krasnoyarsk, 660041 Russia
[d]Institute of Chemistry and Chemical Technology, Krasnoyarsk Scientific Center, Siberian Branch, Russian Academy of Sciences, Akademgorodok 50, bld. 24, Krasnoyarsk, 660036 Russia
[e]Department of Physics and Astronomy, College of Science, King Saud University, PO Box 2455, Riyadh 11451, Saudi Arabia
[f]Department of Chemistry, Maharshi Dayanand University, Rohtak, 124001, India
[g]Rennes University, CNRS, ISCR (Rennes Institute of Chemical Sciences) – UMR 6226, F-35000 Rennes, France.

* Correspondence: issaoui_noureddine@yahoo.fr

Abstract

The present study investigates the physicochemical and biological properties of a novel inorganic-organic hybrid material called (2R,5S)-2,5-dimethylpiperazine-1,4-diium dinitrate (RSDPN). This material was synthesized under mild conditions and crystallized to the monoclinic system with space group $P2_1/c$. The organic portion of the structure forms bifurcated N—H…O and weak C—H…O hydrogen bonds with the nitrate anions, resulting in wavy layers parallel to the (100) plane. The integration of organic and inorganic elements in the RSDPN compound is evident through infrared absorption spectroscopy. In order to comprehensively examine the structural, electrical, and biological properties, a DFT approach was employed. Various analysis techniques such as Hirshfeld surfaces analysis (HS), Atoms-In-Molecules (AIM), Reduced Density Gradient (RDG), and Electron Localized Function (ELF) were utilized to visualize and quantify the intermolecular interactions and types of hydrogen bonds that contribute to the stability and cohesion of the structure. The title compound exhibits remarkable stability and strong electrophilic activity, both of which are common characteristics in physiologically active compounds, as indicated by frontier orbital analysis. Thermal examination revealed a two-stage breakdown process where the substance ignites, producing volatile fumes and a dark carbonaceous residue. Molecular docking analysis suggests that RSDPN inhibitors hold potential for the treatment of Parkinson's, schizophrenia, and Alzheimer's disease. Overall, this study provides a detailed experimental and theoretical investigation of the RSDPN compound, shedding light on its physicochemical and biological properties, and highlighting its potential applications in the field of therapeutic intervention for neurodegenerative disorders.

Keywords: Crystal structure; Alzheimer; Schizophrenia; Parkinson; DFT, TG-DTA, Molecular docking.

1. Introduction

The scientific community is constantly looking for novel materials that are more resilient, effective, and intelligent as a result of technological advancements, particularly in the field of nanotechnology. Activities have been carried out in this research environment to synthesize new hybrid materials based on nitrate and semi-organic that can address specific issues in various fields. In a special place among powerful pharmacological chemical molecules are heterocycles [1-5]. The selection of symmetric diamines, more specifically piperazines, is particularly important for obtaining desirable materials because the application prospects largely depend on their characteristics. Its diamines are widely used for the development of key intermediates or drugs whose biological activity encompasses a wide variety of therapeutic areas [6] such as the vasodilator flunarizine, the antihistamine cetirizine, the antibiotic ciprofloxacin. Studies on the structure-activity relationship of these compounds have shown that alterations in the piperazine ring have a major impact on the biological activity. The synergy of piperazine derivatives with inorganic moieties are numerous namely 1-methylpiperazine-1,4-diium bis(nitrate) [7] which has a remarkable trapping capacity with a powerful reducing power, this confirms the functionality of their antioxidant power, trans-2,5-dimethylpiperazine-1,4-diium pentachlorobismuthate(III) [8] exhibiting antioxidant property, indicating that it may be a promising active component in the formulation of cosmetics and also in the field of biomedical applications, 1-ethylpiperazine-1, 4-diium bis(nitrate) [9] interacts better with covid19 than with SARS COV2 demonstrating the great inhibitory capacity of the promoter in the treatment of novel corona virus. As a contribution to the type research of the aforementioned materials, we provide the synthesis and investigation of a hybrid material that incorporates nitric acid as a mineral component and (2R,5S)-2,5-dimethylpiperazine as an organic matrix component. Thus, (2R,5S)-2,5-dimethylpiperazine is a prochiral molecule which presents two enantiotopic nitrogen atoms. This is a privileged motif found in many biologically active compounds, in particular in δ opioid [10, 11] receptor agonists. As a result, after the preparation of the (2R,5S)-2,5-dimethylpiperazine-1,4-diium dinitrate, this paper describes various experimental and theoretical techniques for characterizing this crystalline structure, including thermal analysis, topological analyses, spectroscopic measurements, Hirshfeld surface analysis, AIM, RDG, ELF, MEPS,

HOMO−LUMO and molecular docking. The ab initio Hartree-Fock (HF) level and DFT have developed into effective tools in recent years for studying molecular structure and vibrational spectra. The study of non-covalent interactions and the relationships between function and structure in our work are the basis of the understanding of biological systems. The biological world is often a source of inspiration in the modeling of supramolecular assemblies. The conclusions drawn from this research should give readers a thorough grasp of the compound potential intermolecular interactions and biological activities.

2. Experimentation specifics

2.1 Components and measurements

In order to conduct X-ray diffraction experiments, the RSDPN single crystal is selected based on its dimensions (0.58x0.46x0.23mm) and morphology, which must be prismatic. A Bruker-AXS APEXII diffractometer operating at molybdenum wavelength (λ = 0.71073 Å) is used to capture the data. The SADABS software was used to treat absorption adjustments using the multi-scan method [12]. Just 1195 of the 4126 reflections observed are independent, and 1059 of them had intensity $I > 2\sigma(I)$. The structure was solved using direct methods with the help of the SIR97 program [13], which were subsequently improved with full-matrix least-square methods based on F^2 (SHELXL-97) [14] with the aid of the WINGX program [15]. Using anisotropic atomic displacement parameters, all non-hydrogen atoms were refined. A different map was used to locate every H atom. They were nonetheless geometrically positioned and refined using a riding model, with C—H = 0.97 (methylene), 0.96 Å (methyl), or 0.98 Å (methine), N—H = 0.90 Å (NH_2), and $U_{iso}(H) = 1.2U_{eq}$ (C or N). Table 1 provides an overview of the crystallographic data and the structure improvements. Using the ORTEP [10] and Diamond [16] programs, structure visualizations are created. A multimodule 92 Setaram analyzer running from ambient temperature up to 773 K at an average heating rate of 10 K/min was used for the thermal analysis, and the mass of the simple for TG/DTA was 18.65 mg. IR spectrum was captured using a NICOLET IR 200 FT-IR infrared spectrometer in the 4000−400 cm^{-1} region.

2.2 Theoretical researches

The foundation of a Hirshfeld surface analysis is a 2D graph that summarizes the complex information contained in a structure and a 3D graph that depicts the space region where the molecules come into contact. This allows for the identification of each type of interaction. Software called Crystal Explorer was used to do this analysis [17]. The hybrid B3LYP/6-311++G (d,p) technique was used in conjunction with the Gaussian 09 software package [18] and the GaussView molecular visualization application [19] to accomplish the molecular

geometry optimization and the quantum chemical computations. According to Bader's theory [20], the topological properties in this study were calculated using the Multiwfn program [21]. The Multiwfn multifunctional wave function analyzer was used to do the RDG-NCI analysis, and the VMD molecular visualization tool was used to visualize the results. iGEMDOCK software was used to explore the molecular docking calculation [22]. The basic ligand-protein interactions' total energy value is provided by this program. The structures of the four enzymes are obtained from Protein Data Bank [23]. From the PDB database, eight complexes with ligands and proteins were chosen. PyMOL [24] and the molecular operating environment [25] are used to determine the visual representations of the docked ligands.

2.3 Synthesis of RSDPN and its crystallization

Under ambient temperature settings, the title crystal was created. 1 mmol of (2R,5S)-2,5-dimethylpiperazine (Percent Purity 98%, Melting Point: 115°C to 119°C, Boiling Point: 162°C to 165°C) in 20 mL of water was combined with 2 mmol of HNO_3 (concentration > 86%, pka= -1.37, Melting Point:-41.6°C, Boiling Point:121 °C) in 10 mL of water. The resulting solution was ~~heated to room temperature before being~~ agitated for an hour and filtered. After a few days, the title chemical was produced as colorless single crystals. Schematically, the response can be expressed as follows:

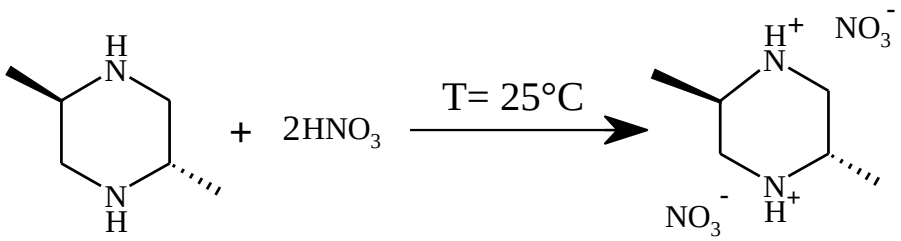

Elemental analysis, calc. (found): C, 29.97% (29.82); H, 6.66% (6.68); N, 23.31% (23.25).

3. Findings and discussion

3.1. Analyzing structure and optimizing geometry

Figure S1 shows the produced compound powder X-ray diffraction pattern. The powder diffractogram exhibits diffraction lines that appear extremely tiny and unwidened, suggesting that the manufactured powder is minuscule. In fact, the lack of further peaks supports the sample's overall purity and the absence of any traces of crystalline impurities.

Figure 1a is an ORTEP representation of the chemical edifice involved in the (2R,5S)-2,5-dimethylpiperazine-1,4-diium dinitrate structure. It shows a nitrate anion and a doubly protonated organic cation. The crystalline stacking of this compound along the $\vec{c}$ axis (Figure 2) shows parallel corrugated layers in x = 0 and x = 1 position which develop in the (b, c)

plane where the organic cations are lodged on either side of the anionic cavities by establishing N−H ... O and C−H ... O weak hydrogen bonds. The three oxygen atoms (O1, O2 and O3) in our structure are considered to be acceptors. The nitrogen atom (N1) of the nitrate anion occupies a general position and forms with these oxygen an ionic molecule adopts the planar trigonal configuration (sp^2 hybridization) with the interatomic bond lengths and angles varying respectively in the ranges [1.2398 (13) –1.2706 (13 Å] and [118.65 (10) –121.73 (10) °]). It is worth noting that the distance N1—O1 is significantly longer than the N1—O2 and N1—O3 distances because O1 is applied in three hydrogen bonds (table1) while O2 and O3 are applied in only one hydrogen bond. These dimensions are also comparable to those observed in the literature [26-29]. Examination of the centrosymmetric group (2R,5S)-2,5-dimethylpiperazine-1,4-diium shows that it is generated by inversion symmetry located at (0, 0, 0) and (0, 1/2, 1/2), it presents a chair conformation with two protonation sites which leads to an increase in the value of the $C2^{i}$ –N2– C1 and $C1^{i}$ – $N2^{i}$ – C2 (Symmetry code: (i) −*x*, −*y*, −*z*) (112.95 °) angles compared to the value observed for, unprotonated Trans-2 5-dimethylpiperazine (108.8 °). This can be explained by engagement of the free doublet of the nitrogen atom in a coordination bond with the transferred proton of nitric acid. The methyl groups occupy equatorial positions with a C1 – C3 distance equal to 1.51 Å. Interatomic bond lengths and angles between the different elements of the cycle of this chair conformation (Figure 2) vary respectively from 1.49 to 1.52 Å and from 109.1 to 112.9 °, with puckering parameters Q = 0.6083 Å , θ = 90 ° and φ = 166 ° [30]. The geometric properties of this cation (Table S1) are in accordance with those previously published in the literature [8, 31]. The characteristics of hydrogen bonds of the title compound are collated in Table 2. Inspection of this table shows the presence of N−H ... O and C−H ... O type hydrogen bonds considered weak according to the Brown and Blessing criterion [32, 33]. Note that H2A and H2B hydrogen atoms are engaged in bifurcated hydrogen bonds as they are the seats of two N−H… O bonds. These bonds vary from 2.8471(14) to 3.2172(14) (Å). The weak C−H… O interactions ensure the junction between the (2R,5S)-2,5-dimethylpiperazine-1,4-diium cations and NO_3^- anions, with a donor-acceptor distance is equal to 3.2614 (14) (Å) relatively long in comparison with those of the N−H… O type. These bonds play an important role in maintaining the crystalline structure of the compound thanks to the rings formed by their combinations $R_1^2(4)$, $R_3^3(9)$, $R_4^4(12)$ and $R_2^1(6)$ (Figure S2) [34].

It has been demonstrated in earlier research that DFT calculations utilizing the B3LYP functional linked to the 6-311++G (d,p) base produce predictions of molecular structures that are consistent with experimental results. Hence, the **RSDPN** structure shown in Figure 1b has

been optimized using the DFT-B3LYP/6-311++G (d,p) approach. In Table S1, the various structural parameters predicted by this **RSDPN** technique are contrasted with those determined by X-ray diffraction. The outcomes demonstrate that these parameters closely match the experimental values. A closer look at the organic cation reveals that the C−C and C−N bonds in this moiety were calculated to be between 1.481 and 1.528 Å, while The C−C−N, C−N−C, and C−C−C bond angles were calculated to range between 108.120 and 113.592 degrees. The predicted average bond length of C−H and N−H is 1.13 Å, which is somewhat longer than the average value of 0.95 Å experimentally observed. The estimated N1−O3 and N1−O4 distances for the nitrate anion are identical to those obtained by X-ray diffraction as long as N1−O2 is extended by 0.03 Å in comparison to the experimental value. This may be explained by the oxygen atom O2 involvement in the hydrogen bond N5−H7…O2. Thus, let's recap the calculations are done in the gas phase, whereas the experimental structure is measured in the crystalline phase, which, in turn, explains why these theoretical errors exist.

This section may be divided by subheadings. It should provide a concise and precise description of the experimental results, their interpretation, as well as the experimental conclusions that can be drawn.

3.2. Visualization and quantification by Hirshfeld surface analysis

Intermolecular interactions observed crystallographically by X-ray diffraction were quantitatively studied and visualized with Crystal Explorer 3.1 by the Hirshfeld surface analysis method. The d_{norm} function is a ratio encompassing the distances of any surface point to the nearest interior (d_i) and exterior (d_e) atom and the van der Waals radii of the atoms. This function displays a well-defined color code, a red color in the negative region where ($d_e + d_i$) is shorter than the sum of the van der Waals radii attributed to the nearest and visualized contacts. The white areas represent the contacts around the van der Waals separation, while the blue spots in the negative part relate to the contacts with ($d_e + d_i$) longer than the sum of the van der Waals radii. The 3D d_{norm} (a) and d_e (b) maps of **RSDPN** recorded in Figure 3 clearly show the presence of large and deep red and orange spots corresponding to the oxygen-hydrogen contacts mainly responsible for the N−H...O hydrogen bonds. The blue and white areas assigned respectively to the H…H and N…H interactions [35, 36]. The percentages of the different contacts and atoms existing in this structure are summarized in Figure 4. In the finger print plots the O···H / H ... O interactions have the greatest contribution on the Hirshfeld surface (60.1%) and appear as two symmetrical wings with a large long point of sum $d_e + d_i$ ~ 1.8 Å less than the sum of the van der Waals radii of the hydrogen (1.09Å)

and oxygen (1.52 Å) atoms (Figure S3a). The H…H contacts comprise 33.6% of the Hirshfeld surface (Figure S3b), this value is very much lower than the value calculated for random contacts (42.51%). In fact the organic part has a large number of hydrogen atoms on their molecular surface (S_H = 65.2%), while carbon atoms are absent on the molecular surface (S_C = 0%) since the piperazinium ring generally lacking double or triple bonds, this confirms the absence of C ... H/H ... C and C ... C contacts on Hirshfeld surface. The rest of the N… H/H… N, O… O and N… O/O… N contacts occupy respectively 3.1%, 1.6% and 1.6% of the Hirshfeld surface. Intermolecular interactions were then assessed by enrichment ratio analysis (ER). The ER values are summarized in Table 3. The list of enrichment ratios highlights the O…H contacts (ER_{OH} = 1.42) which turn out to be favored in the crystal packing, notably the O1, O2 and O3 acceptor atoms and the N2 and C1 donor atoms at the level of the piperazinium ring form four weak hydrogen bonds, three N−H ... O and one C−H ... O. The **RSDPN** compound has very high hydrogen content (S_H = 65.2%) on the Hirshfeld surface, for this reason, according to Jelch's expectation [37], the ER_{HH} enrichment tends, by definition, towards a value close to 1, therefore in our case ER_{HH} equal to 0.80. As long as the H atoms are abundant, the O ... O contacts are very weak (1.6%) resulting in a small enrichment ratio (ER_{OO} = 0.15), this is explained by the oxygen atoms tendency to be involved in N−H ... O and C−H ... O hydrogen bonds.

3.3. NCI-RDG Analysis

In order to study non-covalent interactions (NCI) Johnson et al. [38] proposed the RDG (reduced density gradient) approach. This method provides a graphical visualization of the different interactions existing in the molecule such as hydrogen bonds, van der Waals interactions and repulsive steric interactions. It is a dimensionless quantity, written as follows:

$$RDG(r) = \frac{1}{2(3\pi^2)^{1/3}} \frac{|\nabla\rho(r)|}{\rho(r)^{4/3}}$$

The digital fingerprint (Figure5a) of reduced density gradient as a function of the electron density multiplied by the sign of second eigenvalue of the Hessian matrix allows us to evaluate the bond strength based on the sign $(\lambda_2)^*\rho$. Van der Waals interactions always exhibit very small electron density values ($\rho \approx 0$, $\lambda_2 \approx 0$), whereas regions corresponding to a hydrogen bond ($\rho > 0$, $\lambda_2 < 0$), these obligations appeared with a sign λ_2 ρ ranging from -0.02 to -0.005 Å, or a steric effect ($\rho > 0$, $\lambda_2 > 0$) are associated with high density. Figure5b summarizes the different types of interactions within hybrid material RSDPN, the analysis of this figure shows that the green spots indicate the presence of van der Waals bonds, the elliptical red spots are indicators of the steric effect located at the level of piperazinium rings

reflecting a strong repulsion as well as the light blue spots verified between the hydrogen-oxygen atoms indicate strong attractive N-H...O interactions.

3.4. Atomic and molecular quantum theory

The QTAIM technique ("Quantum Theory of Atoms In Molecules") has been improved by R. Bader [39], this theory makes it possible to characterize the nature of the interatomic interaction between two involved atoms, the non-binding interactions, the electronic structure and the chemical reactivity of the molecule, in particular from the calculation of certain physical properties such as the electron density, Laplacian of the electron density $\blacktriangledown^2\rho(r)$, kinetic energy density G(r), the total energy density H(r) = G(r) + V(r), the potential energy density V(r) and the binding energy E_{bond} = V(r)/2. Locating the electrical density critical spots that match a topological particularity is possible using the AIM technique. The sum of the three eigenvalues of the Hessian matrix makes up the Laplacian of electron density. It is a useful quantity that makes it possible to characterize the ties' nature [40]. If $\blacktriangledown^2\rho(r) < 0$: When we talk about a local charge concentration and for $\blacktriangledown^2\rho(r) > 0$: We refer to this as charge depletion. On the other hand, Rozas et al. [36] offered the following standards to determine the nature of hydrogen bonds:

- A powerful hydrogen bond exists if $\blacktriangledown^2\rho(r) < 0$ and H(r) < 0.
- A moderate hydrogen bond exists if $\blacktriangledown^2\rho(r) > 0$ and H(r) < 0.
- A weak hydrogen bond is one in which $\blacktriangledown^2\rho(r) > 0$ and H (r) > 0.

Using the Multiwfn program, the AIM molecular map of the RSDPN compound is captured in Figure 6a, and the topological parameters of the non-covalent interactions are categorized in Table 4. The calculations' findings indicate that hybrid RSDPN has a BCP between the O2 and H7 atoms that are ascribed to an N−H...O type hydrogen bond (N5−H7...O2). The electron density and the Laplacian are on the order of 0.21 and -0.72 a.u., respectively, at this crucial point. We can observe that its values do not fall into the range of Koch and Popelier, where the electron density and its Laplacian must, respectively, fall within the ranges [0.0020-0.0400 a.u] and [0.024-0.139 a.u]. This can be confirmed by the presence of a remarkably strong hydrogen interaction according to Rozas et al. [41]. In fact, the Laplacian's negative sign at the crucial site of connection denotes a very covalent property. On the other hand, a weakening of the charge in the internuclear area is linked to the positive value of the Laplacian. According to AIM analysis, the BCP at the O...H hydrogen bond is distinguished by an electron density of 0.2 a.u., a negative Laplacian value, a ratio of $|V|/2G) \leq 1$; $G/\rho(r) \geq 1$), and a negative total energy density. We can infer that the N5−H7...O2 hydrogen

bond behaves like a polar-covalent bond from these topological properties. Also take note of the specific description of a crucial point at the piperazinium cycle "RCP" level in this analysis, with positive values for the electron density and the Laplacian, this amply demonstrates the piperazinium nucleus's exceptional stability.

3.5. Molecular electrostatic potential

The molecular electrostatic potential surface (MEPS) is a graphical figuration of the potentials created in the space around a molecule by its electrons and nuclei. This tool makes it possible to identify the electrophilic (regions of positive electrostatic potential) and nucleophiles (regions of negative electrostatic potential) sites and consequently, to know the possibility of formation of intra or intermolecular hydrogen bonds. The molecular electrostatic potential map of the **RSDPN** crystal is illustrated in Figure 6b using a color code where the total electron density varies between two extreme limits: -6.100 $.10^{-2}$ a.u. (dark red) to 6.100.10^{-2} a.u. (dark blue). The red color indicates a strong repulsion, while the blue color indicates a strong attraction and the green indicates a neutral zone (zero potential). This analysis leads to the identification of an enriched zone in electrons (− red) attributed to nucleophilic sites it is mainly located on the oxygen atoms of the NO_3^- group, while the cationic part, particularly the piperazinium ring, has the regions of electrostatic potentials deficient in electrons (+ light blue) relating to the electrophilic sites. With its results one can reach the most reactive nucleophilic and electrophiles sites of the compound which promote the formation of intermolecular hydrogen bonds between the organic and inorganic groups (donor−acceptor interaction).

3.6. Electron localization function (ELF) and localized orbital locator analysis (LOL)

ELF and LOL methods summarize and describe the different types of non-covalent interactions and chemical bonds in 2D graphic maps used in an analysis based on the high conditional probability of finding electron pairs in molecular space [42]. The ELF and LOL color maps are recorded in Figure 7 according to the positions of nuclear atoms in the (x y) and (x z) planes. ELF has a value located in a range between 0.00 and 1.0 subdivided into two sub-domains; the 0.5−1.0 area means that the electrons are strongly localized, while values below 0.5 assigned to the regions where the electrons should be delocalized. So the ELF analysis results show that the blue colored regions around some carbon, nitrogen and oxygen atoms represent the delocalized electron cloud. On the other hand, a strong electronic localization is observed around the hydrogen atoms indicated by the color red: maximum Pauli repulsion. The analysis of the localized orbital locator LOL fingerprint shows the detection of white spots around the hydrogen atoms which indicates that the electron density

exceeds the upper limit of the color scale (0.80). Note that electrons are positioned between all hydrogen and interatomic bonding fields in piperazinium rings (high LOL values). On the contrary, the blue spaces between the two anionic and cationic halves possess small LOL values (0.12 ~ 0.24 a.u.), highlighting the presence of the hydrogen bonds. The results of ELF, LOL and MEPS maps practiced to detect the electrophilic and nucleophilic sites of the synthesized structure agree very well.

3.7. Frontier molecular orbital insight

In order to enhance the synthesized material and detect its reactivity and kinetic stability, we have started the theory of frontier molecular orbitals. HOMO (Highest Occupied Molecular Orbital) and LUMO (Lowest Unoccupied Molecular Orbital) are the most interesting orbitals according to Fukui [43] since they are impeccable indicators of electron displacement in molecular assemblies. The valence (VB) and conduction (CB) bands from HOMO and LUMO respectively are energetically separated by an energy called "gap". These orbitals contribute a major part in the chemical stability of the molecule and play an interesting role in the electrical properties and the UV-visible spectra [44]. Similarly, the gap is very important for the analysis of chemical reactivity and kinetic stability of the structure. A high gap displays an abundant stability of the molecule, on the other hand a low gap compatible with a criterion of high reactivity. The HOMO – LUMO component couple reported in Figure 8 shows that they are positioned respectively on the anionic (NO_3^-) and cationic ($C_6H_{16}N_2^{2+}$) part with a band gap calculated in the gas phase ΔE is in the vicinity of 6.33 eV. This important "gap" is compatible with a high kinetic stability of our RSDPN crystal. Table 5displays the reactivity parameters calculated in the gas phase, related to the energies of the FMOs such as the gap energy, the chemical hardness η, the softness S, the electronegativity χ, the chemical potential μ and the electrophile index ψ according to the relationships already listed below table 6. The calculation results reveal that the title compound has hardness and softness respectively equal to 3.17 eV and 0.31 eV, moreover the index of electrophilicity is about 2.91 eV, it is relatively important so it is a proof to classify our material as being a good electrophile. About chemical potential the negative value (-4.3 eV) is an index of stable and biologically active molecules [45]. These characteristics are often comparable to those in other organic nitrate [46, 47].

3.8. Thermolyses of RSDPN crystal

The differential and thermogravimetric thermal analysis curves of (2R,5S)-2,5-dimethylpiperazine-1,4-diium dinitrate produced using a SETARAM "multimodule 92" type

thermoanalyzer on a sample of mass m = 18.65 mg under an argon atmosphere, from room temperature up to 773 K with a heating rate of 10 K. min^{-1} are given in Figure 9.

The differential thermal analysis (DTA) curve shows a fine and very intense exothermic peak at 493 K and a series of endothermic peaks at 543, 560 and 604 K, the most important of which is located at 604 K. These numerous peaks are accompanied by a significant loss of mass (87%). All of these phenomena correspond to a thermal decomposition process which takes place in two stages:

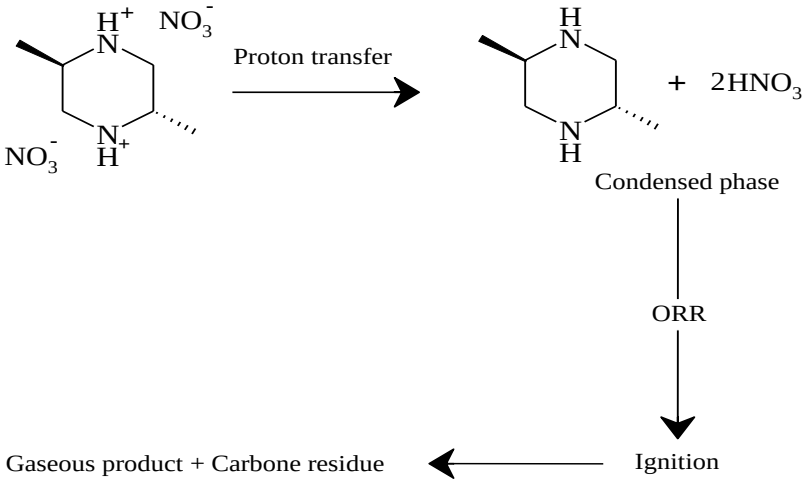

- A first step at 493 K: during this step it was observed a transfer of proton between the ammonium ion and the nitrate anion in a condensed phase and at a higher temperature which causes an internal oxidation−reduction reaction between trans-2,5-Dimethylpiperazine and nitric acid; this leads to inflammation of the material [7, 46,47].
- A second stage starts from 502 K up to 773 K: This stage corresponds to the rest of the decomposition mechanism which has not yet been uniquely defined and different reactions can be assumed [48, 49].

3.9. Molecular docking approach

In order to study the biological properties, especially pharmacological of the elaborate material, we have started modeling by molecular docking, it is a powerful method widely manipulated to discover the activities of the interactions of therapeutic ligands with enzymes. The exact origin of these ailments is still unclear, it is in this context that we tested our compound, which is half organic, belongs to the piperazine derivatives as inhibitors of the proteins associated with Alzheimer's, Schizophrenia and Parkinson's diseases. Recent research efforts show that these proteins B monoamine oxidase (2V5Z), Cyclin-dependent Kinase 2

(1B39), inducible nitric oxide synthase (1DD7) and dopa decarboxylase (1JS3) are interesting targets for the evolution of a new drug against disease [50-53]. The structure of the proteins was taken from the Protein Data Bank (PDB). Molecular docking simulations were applied using iGEMDOCK, MOE.10 and pyMOL software. The calculation results give the opportunity to have ten ligand positions within the active site of each protein whose best position has the lowest energy, and it corresponds to the most stable complex. These best positions are presented in cartoon helix cylindrical mode in Figure. 10. Details of the calculation of conformational interaction energies such as total energy scores, hydrogen bond energies and VDW interactions are collected in Table 6. Examination of this table leads to the following results: the total energy scores are equal to -86.8808; -86.4472; -84.8447 and -79.6866 kcal/mol for the RSDPN inhibitor interacting respectively with the AAAD, iNOS, MAO-B and CdK2 proteins. A predominant major contribution of VDW interactions which are of the order -42.2461, -48.331, -48.2136 and -40.9552 kcal/mol. Regarding the energies of hydrogen bonds have an average value in the vicinity of 39 kcal/ mol. In addition, the analysis of Table S2 reveals that the values of the root mean square deviation (RMSD) of this compound in each system vary from 0.8269 (AAAD) to 3.3872 Å (CdK2), therefore since its values are less than three [54] so they facilitate the stability of the system and confirm the reliability of our docking results [55]. As long as the binding energy scores values are respectively of the order of -5.0631, -4.9329, -4.4587 and -4.8529 kcal/mol for the AAAD, iNOS, MAO-B and CdK2 enzymes. Visual inspection of the two-dimensional maps (Figure 11 and Table S3) of the RSDPN ligand in the active sites of the proteins used along this analysis reveals that the O2, C1 and N2 atoms are related respectively to B: ARG17 (-1.9 kcal/mol), A: GLU150 (-2.6 kcal/mol) and A: ASP310 (-4.8 kcal/mol) residues of the AAAD enzyme by establishment of the classical interactions of hydrogen and ionic bonds, in a distance interval comprised between 2.78 and 3.34 Å. Concerning the observed interactions between the RSDPN inhibitor and the active sites of iNOS (Figure. S4), the A: TRP75, ILE82, ARG84 and C: ASN30 residues respectively form hydrogen bonds with the O1, O2, O2 and C3 atoms where the distances are equal to 2.58, 2.92, 2.95 and 2.66 Å. Also the A: TRP75 residue is engaged in an H-pi interaction with the C1 carbon with a distance of the order of 4.34 Å. Moreover for the third protein our material is surrounded by two amino acids B: THR194 and B:GLU481 respectively generating a hydrogen bond and an ionic interaction having distances equal to 2.75 and 3.21 Å. Finally, the anchored CdK2 conformation (Figure. S6) shows the existence of four conventional hydrogen bonds linked to O2 and N2 atoms (A: THR14 / 3.14 Å; B: ASP84 / 3.10, 3.09 Å; B: ALA101 / 2.74 Å) and an ionic interaction N2−

B: ASP84 / 3.09 Å. So in conclusion based on previous work [50-53], from the energy scores and all the results discussed above, we can consider our ligand as a promising inhibitor in the treatment of Alzheimer's, schizophrenia and Parkinson's diseases since they penetrate well in the active areas of the receptors.

3.10. FT-IR spectral analysis

We conducted a vibratory research utilizing infrared spectroscopy at room temperature to ascertain the vibrational properties of our crystal structure. Table 7 includes a preliminary identification of the observed bands as well as the experimental infrared wavenumber in comparison to the estimated from DFT method assigned by the VEDA program [56] and Gauss View software [14]. Figure 12 depicts the experimental IR spectrum in accordance with the estimated data. We have assigned the various vibration modes of the nitrate anion (NO_3^-) and the organic cation to the set of bands that emerged in the IR spectrum using the assignment results and the bibliographic study [8, 57-63].

- Nitrate anion vibrations

Work on nitrates [45, 47] enabled us to distinguish the four domains of valence vibrational modes and their separation into deformation modes. Four atoms make up the planar trigonal NO_3^- anion, which has (4x3) - 6 = 6 vibrational modes. Asymmetrical elongation mode (ν_1, A'_1, Raman), out-of-plane deformation mode (ν_2, A''_2, IR), doubly degenerate mode of asymmetric elongation (ν_3, E', IR and Raman), and doubly degenerate mode of deformation in the plane (ν_4, E', IR and Raman) are the four subsets of these six vibration modes. The numerous hypotheses for the NO_3^- grouping's symmetrical and asymmetrical vibration frequency assignments are found in the spectral area between 1700 and 1070 cm^{-1}, whereas deformation vibration in and out of plane is recorded between 1070 and 640 cm^{-1}. In this instance, the measured IR spectrum shows the stretching vibrations $\nu_{as}(NO_3^-)$ at 1387 and 1300 cm^{-1}. The DFT approach predicts the same stretching vibrations at 1505 and 1430 cm^{-1}. At 1046 and 1070 cm^{-1}, respectively, additional stretching vibrations $\nu_s(NO_3^-)$ were seen experimentally and theoretically. The band that is associated to the outside plane deformation mode of the NO_3^- group and is experimentally situated towards 977 cm^{-1} has a theoretical estimated value of 778 cm^{-1}. Lastly, in the spectral region between 752 and 554 cm^{-1}, the mode $\nu_4(NO_3^-)$ may be seen. These values match those calculated at 753 and 598 cm^{-1} rather well.

- (2R,5S)-2,5-dimethylpiperazine-1,4-diium vibrations

Heteroaromatics containing N−H groups shows its N−H stretching absorption at [3057−2852 cm-1]. The frequency of these bands is given from the DFT calculations at [3156−2964 cm^{-1}]

range. At the region of 2772 and 2430 cm^{-1}, which correspond to the $-CH_2$ and $-CH_3$ groups, the symmetric and asymmetric stretching of C−H is seen experimentally. By using the DFT level, the same vibrations are estimated at 2945 and 2678 cm^{-1}. The N−H bending mode of NH_2^+ is responsible for the prominent peak located at 1579 cm^{-1}. The corresponding bands are calculated at 1666 cm^{-1}. In effect the $-CH_2$ and $-CH_3$ groups exhibit experimental deformation vibrations in the range 1474−1300 cm^{-1} and calculated in the 1430 to 1281 cm^{-1} frequency range. The experimental spectrum at 1126 and 1046 cm^{-1} show absorptions that are related to the (C−N) and (C−C) stretching vibrations. The vibration at 977 cm^{-1} clearly shows that C−H bending of piperazine is present. These vibrations are calculated respectively by DFT method around 1195, 1144 and 1070 cm^{-1}. Ultimately, the experimental peaks at [946−450 cm^{-1}] domain proved that CCN and CNC deformation were present, respectively. The latter are theoretically provided in the spectral range between 796 and 598 cm^{-1}.

- N−H…O hydrogen bond vibrations

The perturbed NH_2^+ group vibration of the diprotonated (2R,5S)-2,5-dimethylpiperazine-1,4-diium cation is a manifestation of weak N−H…O bonds (2.8471(14)−3.2172 (14) Å) in the vibrational spectrum. So N−H…O stretching vibration is thought to be responsible for the broad band that located between 3240 and 2610 cm^{-1} in the experimental IR spectrum.

4. Conclusions

The slow evaporation approach was used to generate an organic-inorganic single crystal of (2R,5S)-2,5-dimethylpiperazine-1,4-diium dinitrate**.** In a monoclinic system with the $P2_1/c$ space group, this chemical formed crystals. (2R,5S)-2,5-dimethylpiperazine-1,4-diium cation and NO_3^- anions are coupled by N(C)−H... O hydrogen bonds to form a three-dimensional network in the atomic arrangement. It is clear from the information above how the compound many physicochemical and biological features work. Hirshfeld molecular surface analysis reveals the percentage of intermolecular contacts in the molecule, demonstrating that H…O/O…H and H…H interactions are the most significant factors in stabilizing the crystal packing. The optimization findings indicated that the B3LYP functional with a 6−311++G** level is sufficient to investigate the physicochemical characteristics of **RSDPN**. Theoretical and experimental results showed good agreement. The nature and characteristics of molecular interactions are determined via AIM, ELF, LOL, and RDG methods. The behavior of the **RSDPN** reactant in electrophilic and nucleophilic reactions was predicted using the molecular electrostatic potential (MEPS). The outcomes observed are consistent with hydrogen-bond interactions occurring within molecules. Our material exhibits exceptional kinetic stability and biological activity, as evidenced by the HOMO−LUMO energy difference and chemical

potential, which are 6.33 eV and −4.3 eV orders, respectively. The TG−DTA analysis shows that the RSDPN crystals are stable up to 475 K, beyond which they immediately go through a decomposition that happens in two phases and causes our sample to explode and ignite. Concerning infrared spectroscopy, it has been precisely assigned and studied to the vibrational wavenumbers of the core modes of RSDPN. The NO_3^- group's asymmetric stretching mode is responsible for the strong bands between 1450 and 1280 cm^{-1}, and the bands in the 3240−2610 cm^{-1} frequency range are attributed to the stretching modes N-H...O. Molecular docking studies, reveals that the RSDPN inhibitor discovers vital information in the development of medications for the treatment of Parkinson's, Schizophrenia, and Alzheimer's disorders. The conclusions drawn from this work will give readers a precise and thorough understanding of the compound potential intermolecular interactions and biological activities.

Acknowledgements

This work was supported by the Tunisian National Ministry of Higher Education and Scientific Research and Researchers Supporting Project number (RSP2023R61), King Saud University, Riyadh, Saudi Arabia.

References

[1] M. Arshad, K.Ahmed, M. Bashir, N.Kosar, M. Kanwal, M. Ahmed, H.Ullah.Khan, S. Kahn, A. Rauf, A. Waseem, T. Mahmood, Synthesis, structural properties and potent bioactivities supported by molecular docking and DFT studies of new hydrazones derived from 5-chloroisatin and 2-thiophenecarboxaldehyde, J. Mol. Struc 1246 (2021) 131204.[https://doi.org/10.1016/j.molstruc.2021.131204]

[2] A. Allangawi, M. A. Aziz.Aljar, K.ayub, A. Abd El Fattah, T. Mahmood, Removal of methylene blue by using sodium alginate-based hydrogel; validation of experimental findings via DFT calculations, J. Mol. Struc 122(2023) 108468.[https://doi.org/10.1016/j.jmgm.2023.108468]

[3] A. Allangawi, H. Sajid, K.ayub, M. Amjed. Gilani, M. Salim.Akhter, T. Mahmood High drug carrying efficiency of boron-doped Triazine based covalent organic framework toward anti-cancer tegafur; a theoretical perspective, J. Mol. Struc 1220(2023) 113990.[https://doi.org/10.1016/j.comptc.2022.113990]

[4] M. Hanif, N. Kosar, T. Mahmood, M. Muhammad, F. Ullah, M. Nawaz.Tahir, A. Ingrid.Ribeiro, E. Khan, Schiff Bases Derived from 2-Amino-6-methylbenzothiazole, 2-Amino-5-chloropyridine and 4-Chlorobenzaldehyde: Structure, Computational

Studies and Evaluation of Biological Activity, Chem. Phys. Chem 7(2023) 202203386. [https://doi.org/10.1002/slct.202203386]

[5] S. Ahmad , T. Mahmood , M. Ahmada , M. Nadeem. Arshad, F. Ullah, M. Shafiq, S. Aslam, A. M. Asiri, Synthesis, single crystal X-ray, spectroscopic and computational (DFT) studies 2,1-benzothiazine based hydrazone derivatives, J. Mol. Struc 1230(2021) 129854.[https://doi.org/10.1016/j.molstruc.2020.129854]

[6] J. A. Bender, N. A. Meanwell, T. A. Wang, synthesis of diketones from carbonyl compounds and α,ω-dichloro-α,ω-disulfinylalkanes with two carbon–carbon bond-formation via bis-sulfinyloxiranes, Tetrahedron, 58 (2002), 3111.[https://doi.org/10.1016/S0040-4020(02)00352-6]

[7] S. Gatfaoui, A. Mezni, T. Roisnel, H. Marouani, Synthesis, characterization, Hirshfeld surface analysis and antioxidant activity of a novel organic-inorganic hybrid material 1-methylpiperazine-1,4-diium bis(nitrate), J. Mol. Struct., 1139 (2017) 52-59.[https://doi.org/10.1016/j.molstruc.2017.03.028]

[8] M. Essid, M. Rzaigui, H. Marouani, Synthesis, characterization and antioxidant activity of a novel organiceinorganic hybrid material trans-2,5-dimethylpiperazine-1,4-diium pentachlorobismuthate(III): $[C_6H_{16}N_2]BiCl_5$, J. Mol. Struct. 1117 (2016) 257-264. [https://doi.org/10.1016/j.molstruc.2016.03.051]

[9] S. Gatfaoui, A. Sagaama, N. Issaoui, T. Roisnel, H. Marouani, Synthesis, experimental, theoretical study and molecular docking of 1-ethylpiperazine-1,4-diium bis(nitrate), Solid State Sci., 106 (2020), 106326.[https://doi.org/10.1016/j.solidstatesciences.2020.106326]

[10] W. J. Janetka, M. S.Furness, X. Zhang, A. Coop, J. E. Folk, M. V. Mattson, A. E. Jacobson, K. C. Rice, Enantioconvergent synthesis of (-)-(2R,5S)-1-allyl-2,5-dimethylpiperazine, an intermediate to δ-opioid receptor ligands, J. Org. Chem., 68 (2003), 3976.[https://doi.org/10.1021/jo0300385]

[11] K. J. Chang, G. C. Rigdon, J. L. Howard, R. W. McNutt, A novel potent and selective nonpeptidic delta opioid receptor agonist BW373U86, J. Pharmacol. Exp. Ther. 267 (1993), 852.[https://pubmed.ncbi.nlm.nih.gov/8246159/]

[12] Bruker, APEX2, SAINT and SADABS, Bruker AXS Inc, Madison, Wisconsin, USA, 2006.

[13] A. Altomare, M.C. Burla, M. Camalli, G.L. Cascarano, C. Giacovazzo, A. Guagliardi, A.G.G. Moliterni, G. Polidori, R. Spagna, SIR97: a new tool for crystal structure

determination and refinement, J. Appl. Cryst. 32 (1999) 115. [https://doi.org/10.1107/S0021889898007717]

[14] G.M. Sheldrick, Crystal structure refinement with SHELXL, Acta Cryst. C 71 (2015) 3–8. [https://doi.org/10.1107/s2053229614024218]

[15] L.J. Farrugia, WinGX and ORTEP for windows: an update, J. Appl. Cryst. 45 (2012) 849–854.[https://doi.org/10.1107/S0021889812029111]

[16] K. Brandenburg, Diamond Version 2.0 Impact, GbR, Bonn, 1998.

[17] S.K. Wolff, D.J. Grimwood, J.J. McKinnon, D. Jayatilaka, M.A. Spackamn, Crystal Explorer 3.1, University of Westren Australia, Perth, 2013.

[18] M.J. Frisch, et al., GAUSSIAN 09, Revision A.02, Gaussian, Inc., Wallingford, CT, 2009.

[19] R.I. Dennington, T. Keith, J. Millam, GaussView, Version 5.0.8, Semichem. Inc, Shawnee Mission, KS, 2008.

[20] P. S. V. Kumar, V Raghavendra, and V. Subramanian, Bader's Theory of Atoms in Molecules (AIM) and its Applications to Chemical Bonding, J. Chem. Sci. 128, (2016), 1527–1536.[DOI 10.1007/s12039-016-1172-3]

[21] T. Lu, F. Chen, Multiwfn: a multifunctional wavefunction analyzer, J. Comput. Chem. 33 (2012) 580–592.[https://doi.org/10.1002/jcc.22885]

[22] J.-M. Yang, C.-C. Chen, GEMDOCK: a generic evolutionary method for molecular docking proteins, Struct. Funct. Bioinforma. 55 (2004) 288-304.[https://doi.org/10.1002/prot.20035]

[23] http://www.rcsb.org/pdb/.

[24] W. L. DeLano, PyMOL. (2002).

[25] Molecular Operating Environment (MOE), 2015.10; Chemical Computing Group Inc., 1010 Sherbooke St. West, Suite #910, Montreal, QC, Canada, H3A 2R7, 2015.

[26] S. Gatfaoui, H. Marouani, M. Rzaigui, 4-Methylbenzylammonium nitrate, Acta Cryst(2013). E69, o1453.[https://doi.org/10.1107/S1600536813022836]

[27] S. Gatfaoui, H. Marouani, M. Rzaigui, 1,1,4,7,7-Pentamethyldiethylenetriammonium trinitrate, Acta Cryst(2014). E70, o198.[https://doi.org/10.1107/s1600536814001469]

[28] S. Gatfaoui, H. Dhaouadi, T. Roisnel, M. Rzaigui, H. Marouani, m-Xylylenediaminium dinitrate, Acta Cryst (2014) E70, o398–o399.[http://dx.doi.org/10.1107/S1600536814004620]

[29] S. Gatfaoui, H. Marouani, T. Roisnel, H. Dhaouadi, Dopaminium nitrate, Acta Cryst (2014) E70, o571–o572.[http://dx.doi.org/10.1107/S1600536814008265]

[30] D. Cremer, J.A. Pople, A general definition of ring puckering coordinates, J. Am. Chem. Soc. 97 (1975) 1354-1358.[https://doi.org/10.1021/ja00839a011]

[31] C. B. Mleh, T. Roisnel, H. Marouani, *trans*-2,5-Dimethylpiperazine-1,4-diium bis(perchlorate) dihydrate: crystal structure and Hirshfeld surface analysis, Acta Cryst (2016) E72, 593–596.[http://dx.doi.org/10.1107/S205698901600520X]

[32] I. D. Brown, Acta Cryst, (1976) A32, 24.[https://doi.org/10.1107/S0567739476000041]

[33] R. H. Blessing, Acta Cryst, (1986) B42, 613.[https://doi.org/10.1107/S0108768186097641]

[34] J. Bernstein, R.E. Davis, L. Shimoni, N.L. Chang, Patterns in hydrogen bonding: functionality and graph set analysis in crystals, Angew. Chem. Int. Ed. Engl. 34 (1995) 1555- 1573.[https://doi.org/10.1002/anie.199515551]

[35] S. Gatfaoui, N. Issaoui, T. Roisnel, H. Marouani, A proton transfer compound template phenylethylamine: Synthesis, a collective experimental and theoretical investigations, J. Mol. Struc 1191 (2019) 183-196.[https://doi.org/10.1016/j.molstruc.2019.04.093]

[36] S. Gatfaoui, N. Issaoui, S. A. Brandan, T. Roisnel, H. Marouani,Synthesis and characterization of p-xylylenediaminium bis(nitrate).Effects of the coordination modes of nitrate groups on their structuraland vibrational properties,J. Mol. Struc 1151 (2018) 152-168.[https://doi.org/10.1016/j.molstruc.2017.09.027]

[37] C. Jelsch, K. Ejsmont, L. Huder, The enrichment ratio of atomic contacts in crystals, an indicator derived from the Hirshfeld surface analysis, IUCrJ 1 (2014) 119-128.[https://doi.org/10.1107/s2052252514003327]

[38] E.R. Johnson, S. Keinan, P. Mori-Sánchez, J. Contreras-García, A.J. Cohen, W. Yang, J. Am. Chem. Soc. 132 (2010) 6498–6506.[https://doi.org/10.1021/ja100936w]

[39] R.F.W. Bader, Atoms in Molecules: A Quantum Theory, Oxford University Press, Oxford, (1990).[https://doi.org/10.1002/ange.19921041040]

[40] T. Kaharu, R.I. shii, T. Adachi, T. Yoshida, S. Takahashi, J.Mater, Chem. 5 (1995) 687. [https://doi.org/10.1039/JM9950500687]

[41] I. Rozas, I. Alkorta, J. Elguero, Behavior of ylides containing N, O, and C atoms as hydrogen bond acceptors, J. Am. Chem. Soc. 122 (2000) 11154-11161.[https://doi.org/10.1021/ja0017864]

[42] B. Silvi, A. Savin, Classification of chemical bonds based on topologic analysis of electron localization functions, Nature 371 (6499) (1994) 683–

686.[https://ui.adsabs.harvard.edu/link_gateway/1994Natur.371..683S/doi:10.1038/371683a0]

[43] K. Fukui, Theory of Orientation and Stereoselection, Springer-Verlag Berlin Heidelberg, New York, 1975.

[44] I. Fleming, Frontier Orbitals and Organic Chemical Reactions, Wiley, London, 1976.[DOI:10.1002/9780470689493]

[45] M. Salihovic, S. Huseinovic, S. Spirtovic-Halilovic, A. Osmanovic, A. Dedic, Z. Asimovic, D. Zavrsnik, DFT study and biological activity of some methylxanthines, Bull. Chem. Technol. Bos. Herzeg. 42 (2014) 31–36.

[46] S. Gatfaoui, N. Issaoui, S. A. Brandan, M. Medimagh,O. Al-Dossary, T. Roisnel, H. Marouani,A. S. Kazachenko,Deciphering non-covalent interactions of 1,3-Benzenedimethanaminium bis(trioxonitrate): Synthesis, empirical and computational study, J. Mol. Struc 1250 (2022) 131720.[https://doi.org/10.1016/j.molstruc.2021.131720]

[47] S. Gatfaoui, N. Issaoui, T. Roisnel, H. Marouani, Synthesis, experimental and computational study of a non-centrosymmetric material 3-methylbenzylammonium trioxonitrate,J. Mol. Struc 1225 (2020) 129132.[https://doi.org/10.1016/j.molstruc.2020.129132]

[48] I.P.S. Kapoor, P. Srivastava, G. Singh, Preparation, characterization and thermolysis of phenylenediammonium dinitrate salts, J. Hazar. Mater. 150 (2008) 687–694.[https://doi.org/10.1016/j.jhazmat.2007.05.022]

[49] S. Cagnina, P. Rotureau, C. Adamo,Study of incompatibility of ammonium nitrate and its mechanism of decomposition by theoretical approach, Chem. Eng. Transac. 31 (2013) 823–828.[https://doi.org/10.3303/CET1331138]

[50] S. Gatfaoui, N. Issaoui,O. Noureddine, T. Roisnel, H. Marouani,Self assembly of a novel Cu(II) complex, $(C_6H_9N_2)_2$[CuCl4]: experimental, computational, and molecular docking survey, J. Iran. Chem. Soci. 18 (2021) 2331–2343.[https://doi.org/10.1007/s13738-021-02195-y]

[51] O. Noureddine, S. Gatfaoui,S. A. Brandan, H. Marouani, N. Issaoui,Structural, docking and spectroscopic studies of a new piperazine derivative, 1-Phenylpiperazine-1,4-diium bis(hydrogen sulfate),J. Mol. Struc 1202 (2020) 127351.[https://doi.org/10.1016/j.molstruc.2019.127351]

[52] O. Noureddine, S. Gatfaoui,S. A. Brandan, A. Sagaama, H. Marouani, N. Issaoui, Experimental and DFT studies on the molecular structure, spectroscopic properties,

and molecular docking of 4-phenylpiperazine-1-ium dihydrogen phosphate, J. Mol. Struc 1207 (2020) 127762.[https://doi.org/10.1016/j.molstruc.2020.127762]

[53] A. Ramalingam, S. Sambandam, M. Medimagh, O. Al-Dossary, N. Issaoui, M. J. Wojcik.Study of a new piperidone as an anti-Alzheimer agent: Molecular docking, electronic and intermolecular interaction investigations by DFT method,J. Kin. Sau. Uni. Scien. 33 (2021) 101632.[https://doi.org/10.1016/j.jksus.2021.101632]

[54] N. Ahmad, A. Farman, S. L. Badshah, A. U. Rahman, H. Rashid, K. Khan, Molecular Modeling, Simulation and Docking Study of Ebola Virus Glycoproteins. J. Mol. Graph. Model. 72 (2017) 266–271.[https://doi.org/10.1016/j.jmgm.2016.12.010]

[55] M. Arshad, K. Ahmed, Z. Iqbal, U. Rashid, M. N. Arshad, A. M. Asiri, T. Mahmood, Synthesis, structural properties, enzyme inhibition and molecular docking studies of (Z)-N'- (1-allyl-2-oxoindolin-3-ylidene) methanesulfonohydrazide and (Z)-N'-(1-allyl-2-oxoindolin- 3-ylidene)-3-nitrobenzenesulfonohydrazide, J. Mol. Struct. 1221(2020). 128880.[https://doi.org/10.1016/j.molstruc.2020.128880]

[56] M.H. Jamroz, Vibrational Energy Distribution Analysis, VEDA 4, Computer Program, Poland, 2004.[https://doi.org/10.1016/j.saa.2013.05.096]

[57] L.M. Novena, S.S. Kumar, S. Athimoolam, Improved solubility and bioactivity of Theophylline (a Bronchodilator drug) through its new nitrate salt analysed by experimental and theoretical approaches, J. Mol. Struct. 1116 (2016) 45-55.[https://doi.org/10.1016/j.molstruc.2016.03.014]

[58] P. Barczynski, M.R. Sitarz, L. Nowaczyk, Katrusiak, Z.D. Szafran, M. Szafran, Structure and spectroscopic studies of 2,3-diethoxycarbonyl-1- methylpyridinium nitrate, J. Mol. Struct. 1035 (2013) 348-357.[https://doi.org/10.1016/j.molstruc.2012.10.067]

[59] S. Aayisha, T.S. Renuga Devi, S. Janani, S. Muthu,M .Raja, S. Sevvanthi, FT, molecular docking and experimental FT-IR, FT-Raman, NMR inquisitions on "4-chloro-N-(4,5-dihydro-1H-imidazol-2-yl)-6-methoxy-2-methylpyrimidin-5-amine": Alpha-2-imidazoline receptoragonist antihypertensive agent, J. Mol. Struct. 1186 (2019) 468-481. [https://doi.org/10.1016/j.molstruc.2019.03.056]

[60] Tintu K. Kuruvilla, S. Muthu, Johanan Christian Prasana, Jacob George, S. Sevvanthi, Spectroscopic (FT-IR, FT-Raman), quantum mechanical and docking studies on methyl[(3S)-3-(naphthalen-1-yloxy)-3-(thiophen-2-yl)propyl]amine, j.molstruc.1175 (2018) 163-174. [https://doi.org/10.1016/j.molstruc.2018.07.097]

[61] S. Muthu, E. Elamurugu Porchelvi, M. Karabacak, A.M. Asiri, Sushmita S. Swathi, Synthesis, structure, spectroscopic studies (FT-IR, FT-Raman and UV), normal coordinate, NBO and NLO analysis of salicylaldehyde p-chlorophenyl thiose-micarbazone, j.molstruc.1081 (2015) 400-4012. [https://doi.org/10.1016/j.molstruc.2014.10.024]

[62] S. Muthu, E. Isac Paulraj, Molecular structure, vibrational spectra, first order hyper polarizability, NBO and HOMO–LUMO analysis of 4-amino-3(4-chlorophenyl) butanoic acid, Solid State Sci., 14 (2012) 476-487. [https://doi.org/10.1016/j.solidstatesciences.2012.01.028]

[63] S. Seshadri, S. Gunasekaran, S. Muthu, S. Kumaresan, R. Arunbalaji, Vibrational spectroscopy investigation using ab initio and density functional theory on flucytosine, J. Raman Spectrosc. 2007; 38: 1523–1531. [DOI: 10.1002/jrs.1808]

Liste of figures

Fig. 11. 2D interactions of **RSDPN** compound with the amino acid residues of 1JS3.

Fig. 12. Theoretical and experimental FT-IR spectrum of **RSDPN** compound.